

- HARTMAN, F. C., SOPER, T. S., NIYOGI, S. K., MURAL, R. J., FOOTE, R. S., MITRA, S., LEE, E. H., MACHANOFF, R. & LARIMER, W. F. (1987). *J. Biol. Chem.* **262**, 3496–3501.
- HOL, W. G. H. (1985). *Prog. Biophys. Mol. Biol.* **45**, 149–195.
- HWANG, J. K. & WARSHEL, A. (1988). *Nature (London)*, **334**, 270–272.
- JANSON, C. A., SMITH, W. W., EISENBERG, D. & HARTMAN, F. C. (1984). *J. Biol. Chem.* **259**, 11594–11596.
- KETTLEBOROUGH, C. A., PERRY, M. A., BURTON, S., GUTTERIDGE, S., KEYS, A. J. & PHILIPS, A. L. (1987). *Eur. J. Biochem.* **107**, 335–342.
- KNIGHT, S., ANDERSSON, I. & BRÄNDÉN, C.-I. (1989). *Science*, **244**, 702–705.
- KNIGHT, S., ANDERSSON, I. & BRÄNDÉN, C.-I. (1990). *J. Mol. Biol.* **215**, 113–160.
- LAING, W. A., OGREN, W. L. & HAGEMAN, R. H. (1974). *Plant Physiol.* **54**, 678–685.
- LARIMER, F. W., LEE, E. H., MURAL, R. J., SOPER, T. S. & HARTMAN, F. C. (1987). *J. Biol. Chem.* **262**, 15327–15329.
- LORIMER, G. (1981). *Biochemistry*, **20**, 1236–1240.
- LORIMER, G., GUTTERIDGE, S. & MADDEN, M. W. (1987). *Plant Molecular Biology*, edited by D. VON WETTSTEIN & N.-H. CHUA, pp. 21–31. New York: Plenum Press.
- LORIMER, G. & HARTMAN, F. C. (1988). *J. Biol. Chem.* **263**, 6468–6471.
- LORIMER, G. & MIZIORKO, H. M. (1980). *Biochemistry*, **19**, 5321–5328.
- LUNDQVIST, T. & SCHNEIDER, G. (1989a). *J. Biol. Chem.* **264**, 3643–3646.
- LUNDQVIST, T. & SCHNEIDER, G. (1989b). *J. Biol. Chem.* **264**, 7078–7083.
- LUNDQVIST, T. & SCHNEIDER, G. (1991). *Biochemistry*, **30**, 904–908.
- MARTIN, P. G. (1979). *Aust. J. Plant. Physiol.* **6**, 401–408.
- MIZIORKO, H. M. & LORIMER, G. (1983). *Annu. Rev. Biochem.* **52**, 507–535.
- NAKAGAWA, H., SUGIMOTO, M., KAI, Y., HARADA, S., MIKI, K., KASAI, N., SAEKI, K., KAKUNO, T. & HORIO, T. (1986). *J. Mol. Biol.* **191**, 577–578.
- NEWMAN, J. & GUTTERIDGE, S. (1990). *J. Biol. Chem.* **265**, 15154–15159.
- NIERZWIICKI-BAUER, S. A., CURTIS, S. E. & HASELKORN, R. (1984). *Proc. Natl Acad. Sci. USA*, **81**, 5961–5965.
- PAL, G. P., JAKOB, R., HAHN, U., BOWIEN, B. & SAENGER, W. (1985). *J. Biol. Chem.* **260**, 10768–10770.
- PIERCE, J. & GUTTERIDGE, S. (1985). *Appl. Environ. Microbiol.* **49**, 1094–1100.
- PIERCE, J., LORIMER, G. & REDDY, G. S. (1986). *Biochemistry*, **19**, 1636–1644.
- RANTY, B., LUNDQVIST, T., SCHNEIDER, G., MADDEN, M., HOWARD, R. & LORIMER, G. (1990). *EMBO J.* **9**, 1365–1375.
- SCHNEIDER, G., BRÄNDÉN, C.-I. & LORIMER, G. (1984). *J. Mol. Biol.* **175**, 99–102.
- SCHNEIDER, G., BRÄNDÉN, C.-I. & LORIMER, G. (1986). *J. Mol. Biol.* **187**, 141–143.
- SCHNEIDER, G., KNIGHT, S., ANDERSSON, I., LINDQVIST, Y., LUNDQVIST, T. & BRÄNDÉN, C.-I. (1990). *EMBO J.* **9**, 2045–2050.
- SCHNEIDER, G., LINDQVIST, Y., BRÄNDÉN, C.-I. & LORIMER, G. (1986). *EMBO J.* **5**, 3409–3415.
- SCHNEIDER, G., LINDQVIST, Y. & LUNDQVIST, T. (1990). *J. Mol. Biol.* **211**, 989–1008.
- SMITH, H. B., LARIMER, F. W. & HARTMAN, F. C. (1990). *J. Biol. Chem.* **265**, 1243–1245.
- SOMERVILLE, R. C. & SOMERVILLE, S. C. (1984). *Mol. Gen. Genet.* **193**, 214–219.
- SOPER, T. S., LARIMER, F. W., MURAL, R. J., LEE, E. H. & HARTMAN, F. C. (1989). *J. Protein Chem.* **8**, 239–249.
- SOPER, T. S., MURAL, R. J., LARIMER, F. W., LEE, E. H., MACHANOFF, R. & HARTMAN, F. C. (1988). *Protein Eng.* **2**, 39–44.
- SUH, S. W., CASCIO, D., CHAPMAN, M. S. & EISENBERG, D. (1987). *J. Mol. Biol.* **197**, 363–365.
- TABITA, F. R. & MCFADDEN, B. A. (1974). *J. Biol. Chem.* **249**, 3459–3464.
- VAN DYK, D. & SCHLOSS, J. V. (1986). *Biochemistry*, **25**, 5145–5156.

*Acta Cryst.* (1991). **B47**, 835–843

## Ordering and Structural Vacancies in Non-Stoichiometric Cu–Al $\gamma$ Brasses

BY E. H. KISI

*Division of Science and Technology, Griffith University, Nathan, Queensland 4111, Australia*

AND J. D. BROWNE

*Department of Mechanical Engineering, University of Newcastle, NSW 2308, Australia*

(Received 13 February 1991; accepted 9 May 1991)

### Abstract

$\gamma$ -Brass structures are based on the cubic packing of 26-atom clusters which have, as concentric subunits, an inner and an outer tetrahedron (IT, OT), an octahedron (OH) and a cuboctahedron (CO).  $\text{Cu}_5\text{Al}_4$  [ $M_r = 679.37$ ,  $P43m$ ,  $a = 8.7046$  (1) Å,  $V = 659.5$  Å<sup>3</sup>,  $Z = 4$ ,  $D_x = 6.846$  Mg m<sup>-3</sup>,  $R_{wp} = 0.051$ ,  $R_B = 0.017$

for 238 powder reflections] is the stoichiometric  $\gamma$  brass of the Cu–Al system and contains two clusters ( $A$ ,  $B$ ) per unit cell. Al atoms occupy a  $4(e)$  (IT) site in cluster  $A$  and a  $12(i)$  (CO) site in cluster  $B$ . Cu atoms occupy the remaining  $4(e)$  (OT),  $6(f)$  (OH) and  $12(i)$  (CO) sites of cluster  $A$  and the two  $4(e)$  (IT, OT) and a  $6(g)$  (OH) site of cluster  $B$ . The structure has considerable solubility for Al and this

0108-7681/91/060835-09\$03.00

© 1991 International Union of Crystallography

paper contains a systematic neutron powder diffraction study of the changes in the  $\text{Cu}_9\text{Al}_4$  structure at 295 K ( $\lambda = 1.376 \text{ \AA}$ ) and 77 K ( $\lambda = 1.500 \text{ \AA}$ ) as Al is added. The structure was found to remain cubic for compositions  $\text{Cu}_{8.93}\text{Al}_{4.08}$ ,  $\text{Cu}_{8.83}\text{Al}_{4.17}$ ,  $\text{Cu}_{8.75}\text{Al}_{4.25}$  and  $\text{Cu}_{8.58}\text{Al}_{4.42}$ . At  $\text{Cu}_{8.30}\text{Al}_{4.58}$  the structure was slightly distorted to an undetermined symmetry. For  $\text{Cu}_{8.03}\text{Al}_{4.68}$  and  $\text{Cu}_{7.55}\text{Al}_{4.80}$  the structure was found to be rhombohedral [ $M_r = 636.57$ ,  $R3m$ ,  $a = 8.7066(1) \text{ \AA}$ ,  $\alpha = 89.74(1)^\circ$ ,  $V = 660.0(1) \text{ \AA}^3$ ,  $Z = 4$ ,  $D_x = 6.406$ ,  $D_m = 6.41 \text{ Mg m}^{-3}$ ,  $R_{wp} = 0.064$ ,  $R_B = 0.025$  for 702 reflections; and  $M_r = 609.31$ ,  $R3m$ ,  $a = 8.6884(1) \text{ \AA}$ ,  $\alpha = 89.78(1)^\circ$ ,  $V = 655.9(1) \text{ \AA}^3$ ,  $Z = 4$ ,  $D_x = 6.170$ ,  $D_m = 6.18 \text{ Mg m}^{-3}$ ,  $R_{wp} = 0.064$ ,  $R_B = 0.027$  for 789 reflections, respectively]. The non-cubic structures contain sufficient structural vacancies to maintain a classical valence content of 88 electrons per unit cell. Refined structures are presented for all of the above compositions, except  $\text{Cu}_{8.30}\text{Al}_{4.58}$ , and the results discussed in terms of current  $\gamma$ -brass stability theories.

### 1. Introduction

The  $\gamma$ -brass region of the Cu-Al alloy system contains, at different Al concentrations, examples of most of the structural features which arouse interest in the  $\gamma$ -brass structures. These include distortions from cubic symmetry and the formation of structural vacancies.

Many  $\gamma$ -brass phases such as  $\text{Cu}_9\text{Al}_4$  show an extensive range of solid solubility. On the current phase diagram (Willey, 1973) stoichiometric  $\text{Cu}_9\text{Al}_4$  lies just outside the low Al limit of the phase field. As excess Al is added, two derivative structures of lower

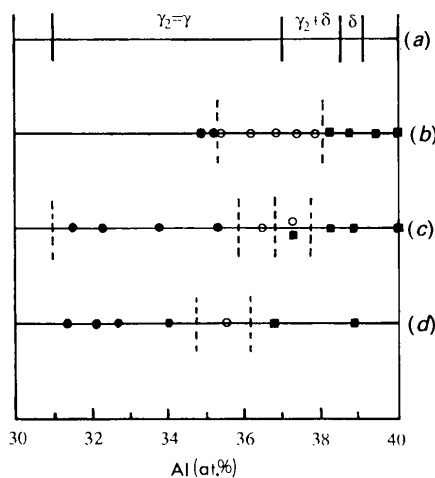


Fig. 1. Room-temperature phase-composition ranges for  $\text{Cu}_9\text{Al}_4$  and derived structures: (a) phase diagram, Willey (1973), (b) Bradley, Goldschmidt & Lipson (1938), (c) Westman (1965b), (d) Kisi (1988). The symbols are:  $\gamma$ -phase structure (●),  $\gamma_1$  structure (○) and  $\gamma_2$  structure (■).

symmetry and fewer atoms per unit cell have been reported (Bradley, Goldschmidt & Lipson, 1938; Westman, 1965b). Their approximate composition ranges at room temperature, shown in Fig. 1, do not conform to those of the current phase diagram. In addition the apparent absence of a two-phase region between cubic  $\text{Cu}_9\text{Al}_4$  and the first derivative structure (Bradley *et al.*, 1938) contravenes the phase rule.

Transmission electron microscopy (TEM) studies (van Sande, van Landuyt, Avalos-Borja, Torres-Villesenor & Amelynckx, 1980) have shown that in air-cooled specimens of 34.6–35 at.% Al the first derivative structure is a metastable long-period inversion-antiphase-domain (IAPD) modification of cubic  $\text{Cu}_9\text{Al}_4$  similar to those characterized by Morton (1974, 1975, 1976, 1979) in Cu-Zn, Pd-Zn, and Ni-Zn  $\gamma$  brasses. However, in alloys cooled at  $6 \text{ K h}^{-1}$ , van Sande *et al.* report that the first derivative structure is replaced by a two-phase mixture of  $\text{Cu}_9\text{Al}_4$  and the second derivative structure. Morton (1987) found the IAPD structure in Cu-Al alloys only at 36 at.% Al and not in alloys with 35 at.% Al. Very fine twinning ( $10 \mu\text{m}$ ) has been observed in alloys having the second derivative structure (van Sande, van Landuyt & Amelynckx, 1979; Lindahl & Westman, 1969).

The stoichiometric  $\gamma$ -brass structures consist of arrangements of clusters of 26 atoms (Fig. 2). Each cluster contains four concentric subunits; these are an inner tetrahedron (IT), an outer tetrahedron (OT), an octahedron (OH) and a cuboctahedron (CO) (Bradley & Thewlis, 1926). In the Cu-Al system, the ideal  $\gamma$ -brass composition is  $\text{Cu}_9\text{Al}_4$ . This structure, the archetypal primitive  $\gamma$  brass, belongs to space group  $P\bar{4}3m$  (No. 215) with two clusters per unit cell,  $A$  at the origin and  $B$  at the cell centre (Bradley, 1928). The subunits IT( $A$ ) and CO( $B$ ) are occupied by the 16 Al atoms with all other sites occupied by Cu atoms.

The structure and the lattice of the first derivative structure have not been determined. The second derivative structure has been reported by Westman

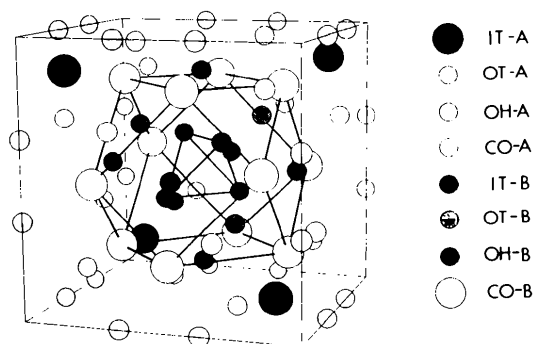


Fig. 2. Ideal  $\text{Cu}_9\text{Al}_4$  structure.

Table 1. *Chemical and physical details of the alloys*

Alloy	Temp. (K)	Lattice parameters		$V_c$ ( $\text{\AA}^3$ )	$D_m$ ( $\text{g cm}^{-3}$ )	Total*	Atoms per unit cell				Ve/cell†
		$a$ ( $\text{\AA}$ )	$\alpha$ (°)				Cu	Total Al	Excess Al	Vacant	
1	295	8.7046 (1)	90.0	659.5 (1)	-	52	35.7	16.3	0.3	0	84.6 (2)
2	295	8.7058 (1)	90.0	659.8 (1)	6.76	52	35.3	16.7	0.7	0	85.4 (2)
3	295	8.7127 (1)	90.0	661.4 (1)	-	52	35.0	17.0	1.0	0	86.0 (2)
4	295	8.7186 (1)	90.0	662.7 (1)	6.62	52	34.3	17.7	1.7	0	87.4 (2)
5	295	8.71 (1)	-	661 (2)	6.52	51.5	33.2	18.3	2.3	0.5	88.1 (2)
6	295	8.7066 (1)	89.74 (1)	660.0 (1)	6.41	50.8	32.1	18.7	2.7	1.2	88.2 (2)
7	295	8.6884 (1)	89.78 (1)	655.9 (1)	6.18	49.4	30.2	19.2	3.2	2.6	87.8 (2)
1	77	8.6782 (1)	90.0								
4	77	8.7032 (1)	90.0								
7	77	8.6728 (1)	89.77 (1)								

\* Corrected by +0.2 for systematic error.

† Total valence electrons per unit cell.

(1965*b*) to have rhombohedral symmetry ( $\alpha = 89.8^\circ$ ), probably of space group  $R3m$  (No. 160), a subgroup of  $P\bar{4}3m$ . A single-crystal structure determination was not reported at this time because of fine-scale twinning (confirmed by the TEM work cited above). A tentative model was later proposed from 'less than satisfactory X-ray data' (Westman, 1972) and is discussed in §4.

This study confirms that structural vacancies which correlate with the total number of valence electrons per unit cell are present in non-cubic Cu–Al alloys with  $\gamma$ -brass derivative structures. The excess Al atoms were found to order to discrete sites in non-stoichiometric cubic  $\gamma$  brasses. In addition, a model is proposed for the rhombohedral derivative structure based on Rietveld refinement of powder neutron diffraction data.

## 2. Experimental

Seven Cu–Al alloys of the compositions shown in Table 1 were induction melted from 99.99% pure starting materials in recrystallized alumina crucibles under a purified argon atmosphere. The alloys were soaked for 10 min in the molten state and cooled slowly in the crucibles. Samples were homogenized for 1 week in evacuated silica ampoules at the temperature indicated in Table 1 and then slowly cooled to room temperature. All alloys appeared uniformly single phase and homogeneity was good when tested by optical microscopy and electron microprobe spot analysis. Twinning was apparent in alloys 6 and 7.

Powders for neutron diffraction were prepared in a tungsten carbide ball mill and had a mean size of 30  $\mu\text{m}$ . Residual stresses were relieved by a vacuum anneal of 4 h at 673 K. The coarsely powdered fraction (75–150  $\mu\text{m}$ ) of alloys 2, 4, 5, 6 and 7 was used for pycnometric density measurements.

Alloys 2 and 7 were chemically analysed by atomic absorption spectroscopy. The measured compositions were in excellent agreement with the nominal compositions shown in Table 1.

Fixed-wavelength neutron powder diffraction data were collected on the Debye–Scherrer-geometry high-resolution powder diffractometer (Howard, Ball, Davis & Elcombe, 1983) at the Australian Nuclear Science and Technology (ANSTO) Lucas Heights laboratory. Monitor-timed scans from 10 to 150 or 160° of  $2\theta$  in steps of 0.05° were collected at room temperature using  $\lambda = 1.376 \text{\AA}$  neutrons from a Ge monochromator. In addition, data were collected at 77 K using a liquid-nitrogen cryostat, for the alloys 1 ( $\lambda = 1.376 \text{\AA}$ ), 4 and 7 ( $\lambda = 1.500 \text{\AA}$ ).

Samples were contained in 16 mm diameter (295 K) or 12 mm (77 K) thin-walled vanadium cans 50 mm high. The containers were rotated (295 K) or oscillated (77 K) to minimize any preferred orientation effects.

X-ray powder diffraction patterns collected on a Philips automated diffractometer operating in the Bragg–Brentano geometry were used to check for phase purity, sample quality and lattice parameters.

## 3. Refinement procedure

Rietveld (1969) analysis of the neutron powder data was carried out using the program *LHPM1* (Hill & Howard, 1986), a modification of the Wiles & Young (1981) program. The Voigt function was selected to model the diffraction peaks. The Lorentz component of the peaks was controlled by a refineable parameter  $\gamma$ , and the Gaussian half-width was modelled by the Caglioti, Paoletti & Ricci (1958) function  $\text{FWHM}^2 = U \tan^2 \theta + V \tan \theta + W$ , where  $U$ ,  $V$  and  $W$  are refineable parameters. Asymmetry was corrected using Howard's method (1982) and the refined parameter  $A$ . Refined peak-shape parameters were always within two standard deviations of the following mean values:  $\gamma = 0.02$ ,  $U = 0.038$ ,  $V = -0.070$ ,  $W = 0.085$  and  $A = 0.16$ . Peak tails were set to zero beyond three half-widths from the calculated peak positions. The scattering lengths used were  $0.3449 \times 10^{-12} \text{ cm}$  for Al and  $0.7689 \times 10^{-12} \text{ cm}$  for Cu. Background scattering was modelled by refining coefficients ( $T_m$ ) in the polynomial  $B_m = T_m(2\theta)^m$

(Wiles & Young, 1981). A  $(1/\sigma_i)^2$  weighting scheme was used where  $\sigma_i$  is the standard deviation of the  $i$ th observation. Measures of the success of refinements used were  $R_p$ ,  $R_{wp}$ ,  $R_B$  and the goodness of fit (GOF) as detailed by Wiles & Young (1981). No preferred orientation effects were detected.

Lattice parameters from the Rietveld refinements were checked by X-ray powder methods for alloys 1, 2, 6 and 7 at room temperature and never differed from them by more than 0.001 Å. This may be taken as an estimate of the accuracy of these parameters. The refinement e.s.d.'s are given in the tabulated presentation of results and these are considered a good estimate of the precision of the determinations compared to others taken at the same neutron wavelength.

Absorption was not a significant factor in these refinements. In each case, the starting model for refinement was that of stoichiometric  $\text{Cu}_9\text{Al}_4$  and the refinements were assumed to have converged when all the parameter shifts were less than 10% of one e.s.d.

Alloys 1–4 were refined in the space group  $P\bar{4}3m$ . For the alloys 6 and 7 the refinements were carried out in the space group  $R3m$  as suggested by Westman (1965a). The relation of the 18 occupied point sets in  $R3m$  to the 8 occupied point sets in  $P\bar{4}3m$  is shown in Table 3. The notation used follows that of Brandon, Pearson, Riley, Chieh & Stokhuyzen (1977). The hexagonal setting was used with the origin fixed at the  $\text{OT}(A)1$  site, the coordinates of which were not refined. The coordinates are reported in the rhombohedral form for easy comparison with the cubic structures.

## 4. Results

### 4.1. Phase boundaries

Alloys 1–4 were found to be cubic whilst alloys 6 and 7 were rhombohedrally distorted. In Fig. 1 the room-temperature phase boundaries from a number of studies of the Cu–Al alloy system are compared with those shown on the current phase diagram. Clearly, the crystal structures of the alloys in this study are not consistent with existing phase boundaries, in that the cubic phase is shown extending to greater Al content than alloy 6. A careful re-evaluation of the phase relationships in this system would therefore seem warranted.

### 4.2. Lattice parameters and density

The alloy details including lattice parameters, densities and the number of atoms of each type per unit cell are shown in Table 1. Also given are the number of Al atoms in excess of the 16 per unit cell of the ideal  $\text{Cu}_9\text{Al}_4$  structure.

The cubic lattice parameter increases with added Al but at a decreasing rate for alloys 1–4. Alloy 5 could not be indexed to any crystal system nor as a cubic + rhombohedral mixture, but the pseudocubic lattice parameter is smaller than for alloy 4. Alloys 6 and 7 continue this downward trend in unit-cell volume with further Al addition. The distortion from cubic ( $0.19$ – $0.24^\circ$ ) is somewhat smaller than that reported for other rhombohedral  $\gamma$  brasses ( $0.5$ – $0.75^\circ$ ) and, surprisingly is larger in alloy 6 than in alloy 7.

Measured densities show an accelerated decline beyond alloy 4 owing to the creation of structural vacancies. At the maximum Al content studied (alloy 7, 38.9 at.% Al) there are 2.6 vacancies and 3.3 excess Al atoms per pseudocubic (rhombohedral) unit cell.

There is a steady increase in the total classical valence-electron count per unit cell up to alloy 4. Within experimental error, the electron concentration is constant at 88 valence electrons per cell for alloys 5, 6 and 7 in agreement with the theory of Jones (1960) concerning the stabilization of non-stoichiometric and defect  $\gamma$  brasses.

In combination, these results confirm the work of Bradley, Goldschmidt & Lipson (1938) but with greater precision as they were only able to resolve pseudocubic unit cells.

The low-temperature measurements indicated that no symmetry changes or phase transformations occur in these alloys on cooling to 77 K.

### 4.3. Al substitution in $\text{Cu}_9\text{Al}_4$

Refinements of atom coordinates and thermal parameters for alloys 1–4 were followed by unconstrained refinement of site occupancies. Substitution of significant amounts of Al for Cu was found on  $\text{IT}(B)$  and  $\text{OH}(B)$  sites for alloys 3 and 4, and at  $\text{IT}(B)$  for alloy 2, but with no clear distinction between these sites for alloy 1. Further refinements constrained the total Al content to be correct for each alloy. The substituting Al was placed on  $\text{IT}(B)$  for alloy 1 because of the behaviour of alloy 2 and extrapolation of the substitutions to an assumed zero at the stoichiometric  $\text{Cu}_9\text{Al}_4$  composition. These results are shown in Table 2.

The refined atom coordinates for the cubic alloys are shown in Table 3. The  $\text{IT}(A)$  (Al) nuclei are displaced 0.043 Å along [111] from the centre of the electron density distribution [X-ray measurements of Arnberg & Westman (1978)]. Significant systematic changes occur in the interatomic distances  $\text{IT}(A)$ — $\text{IT}(A)$  and  $\text{IT}(B)$ — $\text{IT}(B)$ , which increase with increased Al content by a total of 0.128 and 0.044 Å respectively. Thus the two inner tetrahedra grow with excess Al whilst preserving other interatomic distances and cubic symmetry.

Table 2. Models proposed for the non-stoichiometric Cu–Al  $\gamma$  brasses

Rhombohedral site notation is used for all alloys. For the cubic alloys, equivalent sites are given in parentheses.

Alloy	Temp. (K)	CO(A)3 <sup>+</sup>	IT(B)1	IT(B)3	OH(B)3	OH(B)3 <sup>+</sup>
1	295	3Cu	(3.7Cu + 0.3Al)			(6Cu)
2	295	3Cu	(3.4Cu + 0.6Al)		(5.9Cu + 0.1Al)	
3	295	3Cu	(3.4Cu + 0.6Al)		(5.6Cu + 0.4Al)	
4	295	3Cu	(3.3Cu + 0.7Al)		(5.0Cu + 1.0Al)	
4	77	3Cu	(3.1Cu + 0.9Al)		(5.2Cu + 0.8Al)	
6	295	1.7Cu + 1.3Al	0.5Cu	3Cu	2.1Cu	3Cu
7	295	0.8Cu + 2.2Al	Vacant	2.7Cu	1.8Cu	3Cu
7	77	0.6Cu + 2.4Al	Vacant	2.6Cu	1.7Cu	3Cu

Table 3. Atomic coordinates and thermal parameters ( $\text{\AA}^2$ ) of cubic Cu–Al  $\gamma$  brasses

Site	Parameter	Alloy 1, 295 K	Alloy 2, 295 K	Alloy 3, 295 K	Alloy 4, 295 K	Alloy 1, 77 K	Alloy 4, 77 K
IT(A)	<i>x</i>	0.1185 (4)	0.1209 (4)	0.1218 (4)	0.1235 (4)	0.1180 (4)	0.1225 (5)
	<i>B</i>	0.41 (11)	0.52 (12)	0.52 (12)	0.69 (15)	0.11 (10)	0.04 (16)
OT(A)	<i>x</i>	-0.1694 (3)	-0.1700 (3)	-0.1690 (3)	-0.1694 (3)	-0.1701 (3)	-0.1704 (4)
	<i>B</i>	0.60 (7)	0.69 (7)	0.55 (6)	0.63 (7)	0.17 (6)	0.30 (9)
OH(A)	<i>x</i>	0.3556 (3)	0.3549 (3)	0.3549 (3)	0.3551 (4)	0.3554 (3)	0.3556 (4)
	<i>B</i>	0.60 (5)	0.48 (5)	0.57 (5)	0.63 (6)	0.16 (5)	0.31 (7)
CO(A)	<i>x</i>	0.3155 (4)	0.3162 (2)	0.3168 (2)	0.3168 (2)	0.3152 (2)	0.3162 (3)
	<i>z</i>	0.0310 (3)	0.0310 (3)	0.0303 (3)	0.0300 (3)	0.0314 (2)	0.0298 (2)
IT(B)	<i>x</i>	1.04 (3)	0.96 (3)	0.95 (3)	1.02 (6)	0.44 (2)	0.47 (3)
	<i>B</i>	0.6061 (2)	0.6063 (2)	0.6067 (2)	0.6077 (3)	0.6062 (2)	0.6076 (4)
OT(B)	<i>x</i>	0.89 (6)	0.84 (6)	0.84 (6)	1.15 (8)	0.47 (4)	0.79 (10)
	<i>B</i>	0.3254 (3)	0.3255 (3)	0.3247 (3)	0.3250 (3)	0.3258 (3)	0.3256 (4)
OH(B)	<i>x</i>	0.32 (6)	0.28 (5)	0.28 (5)	0.31 (6)	0.12 (5)	0.01 (8)
	<i>B</i>	0.8551 (4)	0.8547 (3)	0.8546 (4)	0.8544 (4)	0.8552 (3)	0.8543 (5)
CO(B)	<i>x</i>	0.76 (6)	0.65 (5)	0.74 (6)	0.63 (6)	0.42 (5)	0.42 (8)
	<i>z</i>	0.8119 (4)	0.8119 (4)	0.8118 (4)	0.8123 (4)	0.8125 (4)	0.8136 (5)
IT(B)	<i>x</i>	0.5330 (5)	0.5328 (5)	0.5320 (5)	0.5318 (6)	0.5332 (5)	0.5320 (7)
	<i>B</i>	0.54 (5)	0.53 (5)	0.39 (5)	0.47 (6)	0.28 (5)	0.34 (6)
IT(B)	<i>R<sub>p</sub></i> (%)	4.03	4.21	4.04	4.65	4.52	5.18
	<i>R<sub>w</sub></i> (%)	5.10	5.18	5.00	5.64	5.28	6.46
IT(B)	GOF	1.90	1.84	1.90	2.24	1.34	1.62
	<i>R<sub>B</sub></i> (%)	1.66	1.47	1.66	1.90	1.37	1.47

Thermal parameters (also shown in Table 3) of the same sites at the same temperature for the various alloys are within one combined e.s.d. of each other with the exception of the IT(B) site. This has a significantly higher *B* value for alloy 4 in both 295 and 77 K measurements, presumably due to the presence of Al on this and the neighbouring OH(B) site. Anisotropic thermal parameters were also refined for the cubic alloys 3 and 4, but the parameters for the CO(B) site were non-positive definite, possibly because of random atom displacements induced by partial Al substitution of the neighbouring IT(B) and OH(B) sites. The refined parameters have been deposited.

Agreement parameters for all four cubic alloys (shown in Table 3) are excellent. Figs. 3(a) and 3(b) are the Rietveld plots for alloys 1 and 4, the least and most Al-substituted respectively. The crosses represent the observed data points, the solid line through them is the calculated profile and the solid line above each is the difference profile on the same scale. Reflection markers are given as vertical bars under each pattern.\*

\* Lists of the observed step-scan neutron diffraction data for alloys 1–7 at 295 K and alloys 1, 4 and 7 at 77 K have been deposited with the British Library Document Supply Centre as Supplementary Publication No. SUP 54216 (37 pp.). Copies may be obtained through The Technical Editor, International Union of Crystallography, 5 Abbey Square, Chester CH1 2HU, England.

#### 4.4. The rhombohedral structure

Initial agreement with the rhombohedrally distorted Cu<sub>9</sub>Al<sub>4</sub> structure was poor (*R<sub>w</sub>* = 14, *R<sub>B</sub>* = 10% for both alloys 6 and 7). Refinement of the atom coordinates and thermal parameters gave very significant improvements but produced many physically unreasonable thermal parameters. Thermal parameters at both 295 and 77 K for the IT(B) site of alloy 7 were so large [9 (1)  $\text{\AA}^2$ ] as to indicate essentially zero scattering from this site. Other large thermal parameters, found at CO(A)3<sup>+</sup>, IT(B)3 and OH(B)3<sup>-</sup>, were taken to indicate either structural vacancies or substitution by excess Al atoms. To quantify the substitutions, the occupancies of CO(A)3<sup>+</sup>, IT(B)3 and OH(B)3<sup>-</sup> were introduced into the refinements.

The models derived from refined occupancies for alloys 6 and 7 are shown in Table 2. Strongly reduced scattering was indicated from all refined sites except IT(B)3 which showed only a small reduction and maintained a large thermal parameter. A fully vacant IT(B)1 site in alloy 7 was confirmed but refinements with this site fully vacant in alloy 6 oscillated and failed to converge. For both alloys 6 and 7, the total reduction in scattering indicated by these occupancies is less than that expected from the unit-cell contents (Table 1). All attempts to locate further sites of Al substitution or vacancy formation

failed, and the large number of parameters involved prevented the use of chemical constraints to enforce the correct Al content. Derivation of a model from these occupancies is difficult because Al substitution and random structural vacancies both produce reduced occupancies during refinements and cannot be uniquely identified. The thermal parameters for the IT( $B$ )3 and OH( $B$ )3<sup>-</sup> sites remain high when the occupancies are refined. When considered in conjunction with the contracted and distorted coordination shells around IT( $B$ )1, IT( $B$ )3 and OH( $B$ )3<sup>-</sup> [compared with that of CO( $A$ )3<sup>1</sup>, which remains much as in the cubic alloys], it is likely that the occupancy changes on the former sites are primarily due to vacancies whilst on the latter to Al substitution.

A somewhat related model was proposed by Westman (1972) with cluster  $A$  as in this model and cluster  $B$  almost identical to  $A$  but with IT( $B$ ) partly vacant. Our data does not support mixed occupancy of CO( $B$ ) but strongly supports the mixed occupancy of OH( $B$ ).

Refined atomic coordinates are given in Table 4 and the relationship to the cubic coordinates is obvious. The expansion of the IT( $A$ ) and IT( $B$ ) groups noted in the cubic alloys continues in the rhombohedral structure. These and other systematic changes in interatomic distances are illustrated in Fig. 4.

Isotropic temperature factors (Table 4) for alloys 6 and 7 remain more erratic than for the cubic alloys but were considered reasonable for a structure

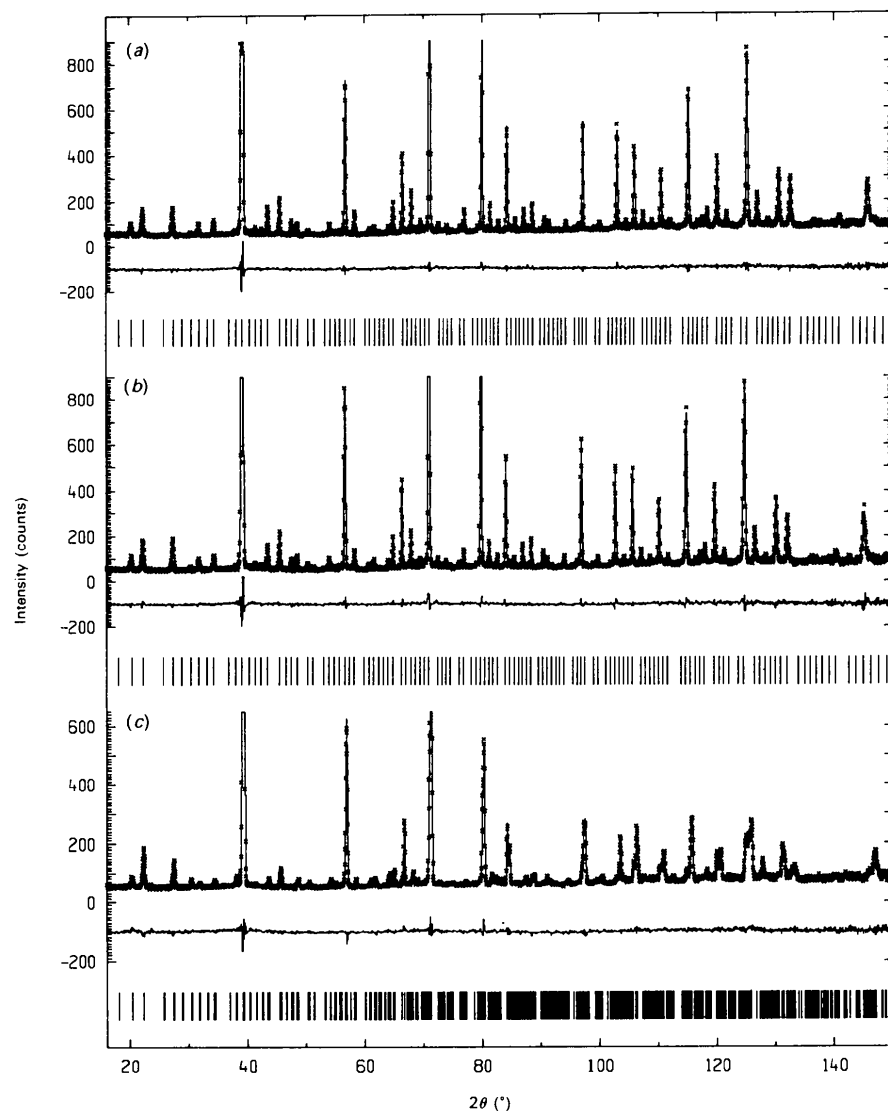


Fig. 3. Plotted output from Rietveld refinements of alloys (a) 1, (b) 4 and (c) 7. The data are shown as crosses and the calculated profiles as solid lines. Difference plots on the same scale and reflection tick marks are given below each fit. The vertical scale has been adjusted to truncate the strong (330, 411) reflection at 25% of its full height to provide a better view of the many weak reflections in these patterns.

Table 4. Atomic coordinates and thermal parameters ( $\text{\AA}^2$ ) of rhombohedral Cu-Al  $\gamma$  brasses

Site	Parameter	Alloy 6, 295 K	Alloy 7, 295 K	Alloy 7, 77 K
IT(A)1	$x = y = z$	0.118 (3)	0.137 (3)	0.134 (3)
	$B$	0.5 (4)	0.6 (5)	0.2 (4)
IT(A)3	$x = z$	-0.138 (3)	-0.129 (3)	-0.126 (3)
	$y$	0.121 (3)	0.118 (3)	0.125 (3)
	$B$	1.1 (5)	0.4 (4)	-0.1 (5)
OT(A)1	$x = y = z$	-0.170	-0.170	-0.170
	$B$	0.9 (3)	1.3 (3)	0.4 (3)
OT(A)3	$x = z$	-0.163 (2)	-0.175 (2)	-0.173 (3)
	$y$	-0.180 (2)	-0.169 (2)	-0.170 (3)
	$B$	0.9 (2)	0.8 (2)	0.4 (2)
OH(A)3 <sup>+</sup>	$x = z$	-0.014 (2)	-0.010 (2)	-0.009 (3)
	$y$	0.344 (2)	0.352 (2)	0.351 (3)
	$B$	0.3 (2)	0.6 (2)	0.7 (2)
OH(A)3	$x = z$	-0.013 (2)	-0.005 (3)	-0.005 (3)
	$y$	-0.367 (2)	-0.356 (3)	-0.357 (3)
	$B$	0.9 (2)	1.2 (3)	0.3 (3)
CO(A)6	$x$	-0.315 (2)	-0.311 (2)	-0.309 (3)
	$y$	0.320 (2)	0.329 (2)	0.333 (3)
	$z$	-0.032 (2)	-0.028 (2)	-0.020 (3)
CO(A)3 <sup>+</sup>	$B$	1.3 (1)	1.2 (1)	0.6 (1)
	$x = z$	0.309 (2)	0.319 (2)	0.320 (3)
	$y$	0.027 (2)	0.029 (2)	0.034 (3)
CO(A)3	$B$	1.0 (3)	0.0 (3)	-0.1 (4)
	$x = z$	-0.330 (2)	-0.325 (2)	-0.323 (3)
	$y$	0.018 (2)	0.027 (2)	0.028 (3)
IT(B)1	$x = y = z$	0.579 (3)	1.3 (3)	0.9 (3)
	$B$	0.6 (5)		
IT(B)3	$x = z$	-0.632 (2)	-0.634 (3)	-0.629 (3)
	$y$	0.607 (2)	0.618 (3)	0.617 (3)
	$B$	2.5 (3)	2.9 (5)	1.9 (4)
OT(B)1	$x = y = z$	0.321 (2)	0.333 (2)	0.330 (4)
	$B$	0.5 (3)	0.4 (2)	0.4 (3)
OT(B)3	$x = z$	-0.335 (2)	-0.331 (2)	-0.326 (3)
	$y$	0.313 (2)	0.323 (2)	0.322 (3)
	$B$	0.7 (2)	1.0 (2)	0.2 (2)
OH(B)3 <sup>+</sup>	$x = z$	0.491 (2)	0.500 (2)	0.501 (3)
	$y$	0.839 (2)	0.847 (2)	0.847 (3)
	$B$	0.3 (2)	-0.1 (2)	-0.1 (2)
OH(B)3	$x = z$	0.493 (3)	0.505 (3)	0.506 (4)
	$y$	-0.869 (3)	-0.859 (3)	-0.857 (4)
	$B$	2.4 (6)	1.4 (5)	1.0 (8)
CO(B)6	$x$	0.814 (2)	0.823 (3)	0.829 (4)
	$y$	-0.817 (3)	-0.811 (3)	-0.806 (5)
	$z$	-0.537 (2)	-0.526 (2)	-0.530 (4)
CO(B)3 <sup>+</sup>	$B$	0.0 (2)	0.1 (2)	0.0 (2)
	$x = z$	0.789 (2)	0.788 (2)	0.794 (3)
	$y$	0.541 (2)	0.547 (3)	0.544 (3)
CO(B)3	$B$	0.5 (3)	-0.2 (2)	-0.3 (4)
	$x = z$	0.829 (3)	-0.818 (3)	-0.819 (3)
	$y$	0.515 (3)	0.522 (3)	0.514 (4)
	$B$	-0.2 (3)	0.3 (4)	0.5 (5)
	$R_p$ (%)	6.40	6.64	6.35
	GOF	6.00	2.5	1.47
	$R_H$ (%)	2.50	2.65	1.93

containing random substitutions and structural vacancies. Anisotropic parameters were not refined.

The  $R$  values for the final rhombohedral structure compare well with those for the cubic alloys. A Rietveld plot is given in Fig. 3(c) for alloy 7.

A structure has not been obtained for alloy 5 as a suitable lattice type could not be determined.

## 5. Discussion

### 5.1. The Cu-Al $\gamma$ brasses

Room-temperature experiments on the cubic alloys (1-4) show that the excess Al goes to the IT(B) site when present in small amounts. At 32.5 at.% Al no further Al is added to the IT(B) site, instead Al substitutes for Cu on the OH(B) site. The 77 K data

confirm this behaviour but with different proportions indicated. It is not known if this difference is systematic, indicating more Al on IT(B) and less on OH(B) in all alloys, or if it is random, indicating that the e.s.d.'s underestimate the uncertainties.

Atomic ordering in the rhombohedral structure differs from that in the cubic structure only on the sites CO(A)3<sup>+</sup>, IT(B)1, IT(B)3 and OH(B)3<sup>-</sup>. These correspond to sites in the cubic alloys where Al substitutes for Cu as well as the Cu site which maintains a large constant temperature factor [CO(A)]. There is, however, some discontinuity in the ordering as a function of composition if the proposed model for alloys 6 and 7 is correct. The Al solution sites in the cubic alloys become partially vacant in the rhombohedral structure whilst most of the excess Al shifts to the CO(A)3<sup>+</sup> site.

Coordination numbers for the different  $\gamma$ -brass sites are difficult to define. Usually, if neighbouring atoms with separations which differ less than 10% from the pure metal radii sums are considered nearest neighbours, IT and OT atoms are 12 coordinated, OH are 13 coordinated and CO atoms are 11 coordinated (with four close next-nearest neighbours). Some of the systematic changes in interatomic distances shown in Fig. 4 occur to compensate for the lowering of coordination resulting from the presence of vacancies. For example, the IT(B)—OT(A) distances which are large in Cu<sub>9</sub>Al<sub>4</sub> are considerably reduced in the rhombohedral structure.

### 5.2. Comparison with other $\gamma$ -brass structures

This work has found no evidence for mixed occupancy of the CO(A) and CO(B) sites as reported in Au<sub>9</sub>In<sub>4</sub> and Cu<sub>9</sub>Ga<sub>4</sub> which have in other respects identical ordering to Cu<sub>9</sub>Al<sub>4</sub> (Brandon, Brizard,

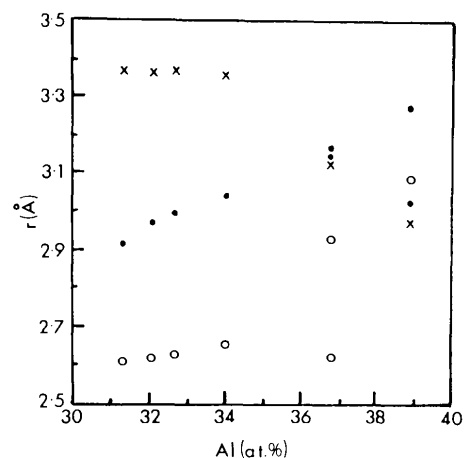


Fig. 4. Interatomic distances IT(A)—IT(A) (●), IT(B)—IT(B) (○) and IT(B)—OT(A) (×) as a function of aluminium content.

Pearson & Tozer, 1977; Stokhuyzen, Brandon, Chieh & Pearson 1974). In the Cu-Al alloys mixed occupancy occurs only to accommodate non-stoichiometric chemical compositions.

The two rhombohedral  $\gamma$  brasses  $\text{Cu}_7\text{Hg}_6$  and  $\text{Cr}_5\text{Al}_8$  that have appeared in the literature (Lindahl & Westman, 1969; Brandon, Pearson *et al.*, 1977) have structures based on the body-centred cubic  $\gamma$  brass ( $\text{Cu}_5\text{Zn}_8$ , clusters *A* and *B* identical) and hence are not directly comparable to  $\text{Cu}_9\text{Al}_4$ . There are, however, some similarities. The mixed occupancy and vacancies occur on the same site types (IT, OT) as in  $\text{Cr}_5\text{Al}_8$  but not in both clusters simultaneously. Also, there is a clustering of structural vacancies towards the negative end of cluster *B* (along [111] of the pseudocubic cell) and the excess Al (larger atoms) is concentrated on the positive end of cluster *A*.

The vacant sites of alloys 6 and 7 are apparently distributed through the structure on several sites. There is only a small contraction of interatomic distances around these sites which are usually partially occupied [except for IT(*B*)1 of alloy 7]. In this respect, and in the loss of cubic symmetry, the Cu-Al alloys 6 and 7 are quite distinct from the transition-metal defect  $\gamma$  brasses  $\text{Ni}_8\text{Cd}_{40}$ ,  $\text{Pt}_8\text{Cd}_{40}$ ,  $\text{Cu}_5\text{NiZn}_{36}$  and  $\text{Pd}_8\text{Cd}_{43}$  which are primitive cubic  $\gamma$  brasses and have 4, 4, 3 and 1 vacant atom sites, respectively (Ljung & Westman, 1970; Arnberg, 1980; Sarah, Rajasekharan & Schubert, 1981). Ordering of the atoms in these phases takes various forms but in all cases the vacancies are confined wholly to the IT(*A*) sites, which in  $\text{Ni}_8\text{Cd}_{40}$  and  $\text{Pd}_8\text{Cd}_{40}$  are fully vacant, accompanied by a partial collapse of cluster *A*. Generally, for less than four vacancies, there are only minor adjustments to interatomic distances.

### 5.3. Theoretical aspects

The  $\gamma$ -brass structure is stabilized with respect to competing structures by electronic energy effects (see, for example, Jones, 1960). The wide range of compositional stability for  $\gamma$ -brass structures in the Cu-Al system was postulated (Bradley *et al.*, 1938) to occur by the formation of structural vacancies in order to keep the number of valence electrons per unit cell constant at 88. It was assumed that this level corresponds to the critical point in the filling of the first 'Jones' zone of the alloy beyond which the  $\gamma$ -brass structure would be unstable. It is just lower than the 90 valence electrons per unit cell required to completely fill the zone. This work confirms such behaviour in the Cu-Al system (Table 1).

Morton (1974, 1975, 1976, 1977, 1979, 1985, 1987) has shown correlations between the mean valence electron concentration (per atom) and the inversion-

antiphase-domain (IAPD) spacing on the electron-deficient side of the  $\gamma$ -brass phase fields of the Cu-Zn, Ni-Zn and Pd-Zn alloy systems. The observations of IAPD structures in Cu-Al alloys at or near the composition of alloy 5 are of particular interest in the light of this. Unfortunately, density measurements did not accompany Morton's work and so the more reliable factor of valence electrons per unit cell cannot be calculated for the alloys used.

Arising from their work with  $\text{Cr}_5\text{Al}_8$ , Brandon, Pearson *et al.* (1977) suggest that in rhombohedral  $\gamma$  brasses a zone splitting occurs which maintains a Fermi surface-Brillouin zone boundary contact in a reduced cell containing 104 valence electrons per unit cell. Increasing the electron concentration would increase the rhombohedral distortion. This does not occur in the Cu-Al alloys which, in addition, contain 88 valence electrons per unit cell.

Brandon, Brizard *et al.* (1977) have claimed that the ordering of atoms in the primitive cubic  $\gamma$  brasses (like  $\text{Cu}_9\text{Al}_4$ ) is controlled by the minimization of like neighbours and maximization of the number of close unlike neighbours. At low excess Al content, these criteria are best met by the OT(*B*) site. However, these measurements have shown that the OT(*B*) site remains fully occupied by Cu and the IT(*B*) and OH(*B*) sites take the excess Al.

It would appear that as yet there is no satisfactory theory to account for the variation in structural details in the Cu-Al  $\gamma$  brasses with composition. There is clearly a need for systematic studies of  $\gamma$ -brass phases in other alloy systems and their variations with composition. It is important that accurate chemical analyses and density measurements are included in the data reported in such work.

One author (EHK) wishes to acknowledge the support of an Australian Institute of Nuclear Science and Engineering (AINSE) studentship during the course of this work. Both authors wish to thank Dr R. L. Davis and other members of the AINSE and ANSTO neutron diffraction group at Lucas Heights for their time and encouragement.

### References

- ARNBERG, L. (1980). *Acta Cryst.* **B36**, 527-532.
- ARNBERG, L. & WESTMAN, S. (1978). *Acta Cryst.* **A34**, 339-404.
- BRADLEY, A. J. (1928). *Philos. Mag.* **7**(6), 878-889.
- BRADLEY, A. J., GOLDSCHMIDT, H. J. & LIPSON, H. (1938). *J. Inst. Met.* **63**, 149-161.
- BRADLEY, A. J. & THEWLIS, J. (1926). *Proc. R. Soc. London Ser. A*, **112**, 678.
- BRANDON, J. K., BRIZARD, R. Y., PEARSON, W. B. & TOZER, D. J. N. (1977). *Acta Cryst.* **B33**, 527-537.
- BRANDON, J. K., PEARSON, W. B., RILEY, P. W., CHIEH, C. & STOKHUYZEN, R. (1977). *Acta Cryst.* **B33**, 1088-1095.
- CAGLIOTI, G., PAOLETTI, A. & RICCI, F. P. (1958). *Nucl. Instrum. Methods*, **3**, 223-228.

- HILL, R. J. & HOWARD, C. J. (1986). Report AAEC/M112. Australian Atomic Energy Commission, Lucas Heights Research Laboratories, Australia.
- HOWARD, C. J. (1982). *J. Appl. Cryst.* **15**, 615–620.
- HOWARD, C. J., BALL, C. J., DAVIS, R. L. & ELCOMBE, M. M. (1983). *Aust. J. Phys.* **33**, 507–518.
- JONES, H. (1960). *The Theory of Brillouin Zones and Electronic States in Crystals*, 1st ed. Amsterdam: North-Holland.
- KISI, E. H. (1988). Thesis, Univ. of Newcastle, NSW, Australia.
- LINDAHL, T. & WESTMAN, S. (1969). *Acta Chem. Scand.* **23**, 1181–1190.
- LJUNG, H. & WESTMAN, S. (1970). *Acta Chem. Scand.* **24**, 611–617.
- MORTON, A. J. (1974). *Phys. Status Solidi A*, **23**, 275–289.
- MORTON, A. J. (1975). *Phys. Status Solidi A*, **31**, 661–674.
- MORTON, A. J. (1976). *Phys. Status Solidi A*, **33**, 395–403.
- MORTON, A. J. (1977). *Phys. Status Solidi A*, **44**, 205–214.
- MORTON, A. J. (1979). *Acta Metall.* **27**, 863–867.
- MORTON, A. J. (1985). Inst. Phys. Conf. Ser. No. 78, ch. 9, p. 343. Bristol: Institute of Physics.
- MORTON, A. J. (1987). Private communication.
- RIETVELD, H. M. (1969). *J. Appl. Cryst.* **2**, 65–71.
- SANDE, M. VAN, VAN LANDUYT, J. & AMELYNCKX, S. (1979). *Phys. Status Solidi A*, **55**, 41.
- SANDE, M. VAN, VAN LANDUYT, J., AVALOS-BORJA, M., TORRES-VILLENOR, G. & AMELYNCKX, S. (1980). *Mater. Sci. Eng.* **46**, 167–173.
- SARAH, N., RAJASEKHARAN, T. & SCHUBERT, K. (1981). *Z. Metall.* **72**(10), 732–735.
- STOKHUYZEN, R., BRANDON, J. K., CHIEH, C. & PEARSON, W. B. (1974). *Acta Cryst.* **B30**, 2910–2911.
- WESTMAN, S. (1965a). *Acta Chem. Scand.* **19**, 1411–1419.
- WESTMAN, S. (1965b). *Acta Chem. Scand.* **19**, 2369–2372.
- WESTMAN, S. (1972). *Chem. Commun. Univ. Stockholm*, **4**, 137.
- WILES, D. B. & YOUNG, R. A. (1981). *J. Appl. Cryst.* **14**, 149–151.
- WILLEY, L. A. (1973). In *Metals Handbook* 8th ed., Vol. 8. Cleveland: American Society for Metals.

*Acta Cryst.* (1991). **B47**, 843–848

## Accurate Structure Analysis with Synchrotron Radiation. An Application to Borazone, Cubic BN

BY K. EICHHORN

*Hamburger Synchrotronstrahlungslabor (HASYLAB) am Deutschen Elektronen-Synchrotron (DESY),  
Notkestrasse 85, D-2000 Hamburg 52, Germany*

A. KIRFEL

*Universität des Saarlandes, FR Kristallographie, D-6600 Saarbrücken 11, Germany*

AND J. GROCHOWSKI AND P. SERDA

*Regional Laboratory, Jagiellonian University, 30-060 Kraków, Karasia 3, Poland*

(Received 24 December 1990; accepted 11 June 1991)

### Abstract

An accurate room-temperature structure analysis has been carried out on borazone, cubic BN, using synchrotron radiation. X-ray diffraction data were collected on the five-circle diffractometer at HASYLAB during dedicated runs (3.7 GeV) of DORIS II at a wavelength of  $\lambda = 0.5000(1) \text{ \AA}$  up to  $\sin\theta/\lambda = 1.45 \text{ \AA}^{-1}$ . Comparison with accurate tube data measured with  $\text{Ag K}\alpha$  radiation [Will, Kirfel & Josten (1986). *J. Less. Common Met.* **117**, 61–71] resulted in a general agreement factor of 0.0135 (0.006 omitting the four lowest-order reflections). Refinements with multipole expansions up to the hexadecapole level yielded  $R$  values as low as 0.0046. The final  $R$  value of a joint data set, prepared by weighted averaging of tube and synchrotron data, was 0.0077. Ensuing deformation density maps agree well with expectation. The analysis and the refinements of the syn-

chrotron radiation data, as well as the comparison with the X-ray tube data, support our previous findings on cuprite,  $\text{Cu}_2\text{O}$ , and corundum,  $\alpha\text{-Al}_2\text{O}_3$  [Kirfel & Eichhorn (1990). *Acta Cryst.* **A46**, 271–284], indicating that high-quality X-ray diffraction data can be obtained at a synchrotron radiation source within normal beam-time allocation.

### 1. Introduction

In a recent feasibility study, accurate room-temperature structure analyses have been carried out on cuprite,  $\text{Cu}_2\text{O}$ , and corundum,  $\alpha\text{-Al}_2\text{O}_3$  (Kirfel & Eichhorn, 1990; hereafter referred to as KE), using synchrotron radiation. This work served to assess the accuracy of single-crystal X-ray diffraction data that can be obtained with such a source. Experimental and data-processing problems were discussed in